International Journal of Applied Mathematics

Volume 38 No. 12s, 2025

ISSN: 1311-1728 (printed version); ISSN: 1314-8060 (on-line version)

THREE – DIMENSIONAL TIME –FRACTIONAL ADVECTION-DIFFUSION MODELING MODELING OF POLLUTANT DISPERSION: ANALYTICAL AND NUMERICAL FRAMEWORK

Shankar Pariyar[1], Bishnu P. Lamichhane[2], Jeevan Kafle[3*], Eeshwar Prasad Poudel[4]

[1] PhD Scholar, Central Department of Mathematics, IOST, T. U., and Faculty of Tri-Chandra Multiple Campus,
Tribhuvan University, Kathmandu, Nepal.
E-mail address: shankar.pariyar@trc.tu.edu.np

[2] School of Information and Physical Sciences, The University of Newcastle, NSW, Australia
E-mail address: bishnu.lamichhane@newcastle.edu.au

[3]Central Department of Mathematics, Kirtipur, Tribhuvan University, Kathmandu, Nepal
E-mail address: jeevan.kafle@cdmath.tu.edu.np

[4] PhD Scholar, Central Department of Mathematics, IOST, T. U., and Faculty of Tri-Chandra Multiple Campus,
Tribhuvan University, Kathmandu, Nepal.
E-mail address: eeshwarpoudel475@gmail.com

[3 *]corresponding author: *E-mail address*: jeevan.kafle@cdmath.tu.edu.np

ABSTRACT

In the study of atmospheric pollutant transport, traditional diffusion models fall short in accurately characterizing sub-diffusive behavior, where particles demonstrate non-Gaussian dispersion and extended retention due to memory effects and anomalous dynamics. To address this limitation, we have developed both analytical and numerical solutions for a three-dimensional time-fractional advection-diffusion equation in the Caputo sense, employing Dirichlet boundary conditions. This approach effectively captures the anomalous transport behaviors and memory-dependent dynamics present in the atmosphere. The analytical solution, obtained through eigenfunction expansion and Laplace transform, results in a closed form that incorporates Mittag–Leffler functions to represent temporal memory effects. Furthermore, a finite-difference method based on the Grunwald–Letnikov discretization was devised to numerically solve the fractional derivative. The proposed scheme's consistency, stability, and convergence were thoroughly evaluated. The simulation results demonstrate that fractional orders within the range $\alpha = 0.5$ to 0.8 significantly improve the precision of the model, achieving absolute error reductions of 42 %- 89% compared to the classical case ($\alpha = 1.0$), particularly at vertical levels below 500 m. Under sub-diffusive conditions, the persistence of pollutant was extended by approximately 30 %- 50%. These findings underscore the efficacy of fractional modeling in precisely describing atmospheric pollutant dispersion.

Keywords: Fractional Partial Differential, Time-Fractional Advection–Diffusion, Three-Dimensional Modeling, Anomalous Pollutant Transport, Mittag–Leffler Functions

Mathematics Subject Classifications: 35Q30, 35R11, 76M12, 76D05, 92E10, 35K57

Received: August 05, 2025

International Journal of Applied Mathematics

Volume 38 No. 12s, 2025

ISSN: 1311-1728 (printed version); ISSN: 1314-8060 (on-line version)

1. Introduction

Modeling atmospheric pollutant dispersion is crucial due to its impact on public health, environmental policy, and climate systems [35, 36, 37]. Conventional methods often struggle to capture the complex dynamics of pollutant transport [1, 2]. Factors such as turbulent wind patterns [38, 39], vertical stratification, and lingering effects from prior emissions challenge the assumptions of classical diffusion models [3, 4]. Overcoming these limitations requires integrating physical processes with advanced mathematical frameworks that accurately reflect real-world dispersion [5, 7]. Among these, the advection-diffusion equation (ADE) remains a fundamental model describing the interaction between atmospheric motion and dispersion driven by concentration gradients [6, 8, 9]. However, classical ADEs do not address phenomena such as sub-diffusion and long-range temporal dependencies [10]. To address this, fractional calculus, which generalizes differentiation to non-integer orders is employed [12, 13]. This approach effectively models memory dependent transport [40], where past atmospheric states influence current pollutant behavior, and captures non-Fickian diffusion [42]. By incorporating inherent spatio-temporal structures, fractional derivatives overcome the shortcomings of traditional integer-order models [15, 40]. Time-fractional derivatives, defined via Caputo or Grünwald–Letnikov formulations, enhance modeling of subdiffusive processes with delayed transport [9, 12], representing particle spread slower than predicted by classical diffusion [16]. Extending the model to three dimensions further improves its ability to represent pollutant concentration variations both vertically and horizontally over time [17, 18]. The 3D time-fractional advection-diffusion equation [41] (3D-TFADE) pro- vides a robust model for pollutant transport, aiding urban planning, environmental monitoring, and public health decisions.

This advancement addresses the shortcomings of traditional modeling approaches [38, 42]. Understanding pollutant dispersion in complex atmospheric systems has long relied on classical advection-diffusion equations (ADEs), which assume Gaussian plume behavior and Fickian transport [35, 39]. However, in real-world environments, especially turbulent and heterogeneous settings, pollutant movement often deviates from these assumptions, exhibiting anomalous dispersion patterns [38]. Three-dimensional time-fractional advection- diffusion models (3D-TFADEs) have emerged as a powerful tool to describe such irregular transport phenomena by incorporating memory and non-local spatial effects [8, 9, 22]. These models effectively overcome the limitations of traditional Eulerian and Lagrangian representations by capturing subdiffusive dynamics, where the plume width evolves with time as t^{α} for $\alpha < 1$, or even superdiffusive with $\alpha \geq 3$, depending on the medium [22, 24, 25]. Fractional calculus has become a powerful tool for capturing the complexities of environmental systems, especially in describing non-standard pollutant dispersion behaviors within heterogeneous media [13, 15]. Continuous time random walks (CTRW), first introduced by Montroll and Weiss (1965) [23], have been widely used to model non-Fickian transport phenomena in diverse media such as

Received: August 05, 2025

International Journal of Applied Mathematics

Volume 38 No. 12s, 2025

ISSN: 1311-1728 (printed version); ISSN: 1314-8060 (on-line version)

fractured rocks, soils, and turbulent atmospheric flows [8, 11, 43]. Berkowitz et al. (1998) [24] advanced this framework by linking CTRW to fractional-order operators, thereby enhancing its theoretical foundation and practical relevance in describing anomalous diffusion processes [35, 44]. The pioneering studies by Podlubny (1999) [21] and Metzler & Klafter (2000) [22] rigorously established the theoretical foundation of fractional calculus for characterizing memory-driven and non-Fickian transport processes, demonstrating its superiority over classical models in capturing anomalous diffusion dynamics [13, 15]. Advancing this framework, Zhang et al. (2017) [30] and Odibat (2023) [20] demonstrated the effectiveness of fractional-order models in capturing gaseous contaminant retention dynamics, while Liu et al. (2019) [31] provided experimental validation in real-world dispersion scenarios. The Caputo fractional derivative is widely favored in environmental modeling because it aligns well with physical initial conditions, reflects observed data trends, and effectively captures memory-driven behaviors, as demonstrated in the works of Chen & Liang (2017) [15] and Ahmed & Haq (2024) [28]. These developments demonstrated the ability of fractional calculus to capture the spatio-temporal correlations present in environmental processes, including pollutant dispersion over complex terrain [17]. Fractional advection-diffusion equations (FADEs) later became widely used in modeling pollutant transport, as studies by Meerschaert et al. (1999) [25] and Deng et al. (1993) [26] highlighted their improved accuracy over classical integer-order models in representing subsurface and surface irregularities [18]. Recent advancements in computational techniques such as wavelet-based solvers (Yadav, 2024) [27], adaptive Grünwald–Letnikov schemes (Ahmed, 2024) [28], and finite element approaches (Gao & Liu, 2023) [29] now allow for efficient handling of complex boundary conditions and terrain-induced turbulence, particularly relevant for regions with complex topography like Kathmandu [45, 47]. These developments establish fractional calculus as a vital framework for high-resolution environmental modeling where classical ADEs often fall short.

Pariyar et al. [9] proposed a 1D time-fractional model for NH_3, CO, and CO_2 dispersion, but it could not capture complex urban topography. Despite these advancements, few studies have explored the full three-dimensional structure of pollutant dispersion using time-fractional models, especially in relation to vertical stratification in the planetary boundary layer. Moreover, the error characteristics and physical interpretations across varying heights and fractional orders remain insufficiently analyzed. The computational challenges associated with solving three dimensional FADEs have also hindered their practical deployment in high-resolution simulations, leaving a critical gap in predictive capability for air quality assessment. This work addresses the gap by developing and analyzing a three-dimensional time-fractional advection-diffusion equation (3D-TFADE) that accounts for anomalous subdiffusive behavior and memory effects in atmospheric transport. We derive an exact analytical solution using separation of variables, Fourier series, and the Mittag-Leffler function, and validate it against a novel finite difference scheme based on the Grünwald– Letnikov approximation. Our

International Journal of Applied Mathematics

Volume 38 No. 12s, 2025

ISSN: 1311-1728 (printed version); ISSN: 1314-8060 (on-line version)

hypothesis is that lower fractional orders $\alpha < 1$ yield improved accuracy in representing real pollutant behavior, particularly in the lower atmosphere. The model is tested across various heights and fractional parameters, with the aim of establishing its accuracy, stability, and physical relevance for environmental applications. By capturing memory effects and non-Fickian transport mechanisms, the proposed 3D-TFADE framework offers substantial improvement over classical models in forecasting pollutant dispersion. The analytical-numerical validation provides insights into plume retention, stratified behavior, and the computational feasibility of fractional modeling. This work contributes not only to the theoretical foundation of fractional transport but also to the development of more reliable and policy-relevant air quality assessment tools. It opens pathways for advanced simulation capabilities in regulatory, urban planning, and environmental health contexts.

The paper is organized as follows: Section 1 presents Introduction, Section 2 covers the basic principles of Fractional Calculus. Section 3 presents the 3D Analytical Plots of Fractional Advection-Diffusion Pollution Dispersion at Various Orders. Section 4 3D Analytical Plots of Fractional Dispersion at Varying Orders. Section 5 Consistency, Stability and Convergence. Section 6 compares the analytical and numerical results to validate the model. Finally, Section 7 highlights the advantages of combining both analytical and numerical methods for environmental modeling.

Nomenclature

C: Pollutant concentration [μg/m^3]

$V^n_{m,l,p}$: Numerical solution at grid point [μg/m^3]

D: Diffusion coefficient [m^2/s]

u_x: Velocity components in x-directions [m/s]

u_y : Velocity components in y-directions [m/s]

u_z: Velocity components in z-directions [m/s]

λ : Decay coefficient [s^{-1}]

Q : Source/sink term [μg/(m^3·s)]

α : Fractional order [dimensionless]

$\partial^\alpha/\partial t^\alpha$:Caputo time-fractional derivative

$E_{\alpha,\beta}$: Mittag–Leffler function

$\Gamma(\cdot)$: Gamma function

L_x : Domain dimensions in x-directions [m]

L_y : Domain dimensions in y-directions [m]

L_z : Domain dimensions in z-directions [m]

Received: August 05, 2025

International Journal of Applied Mathematics

Volume 38 No. 12s, 2025

ISSN: 1311-1728 (printed version); ISSN: 1314-8060 (on-line version)

h_x : Spatial step sizes in x-directions [m]

h_y : Spatial step sizes in y-directions [m]

h_z : Spatial step sizes in z-directions [m]

k : Temporal step size [s]

γ: Separation constant [m^{-2}]

∇^2 : Laplacian operator

Abbreviations

L : Laplace transform operator

FAD : Fractional Advection-Diffusion

ADE : Advection-Diffusion Equation

3D: Three dimensional

PDE : Partial Differential Equation

FPDE : Fractional Partial Differential Equation

CTRW : Continuous Time Random Walk

GL : Grünwald–Letnikov

$PM_{2.5}$: Particulate matter with diameter < 2.5 μm [$\mu g/m^3$]

PBL : Planetary Boundary Layer

MLF : Mittag–Leffler Function

FDM : Finite Difference Method

LTE : Local Truncation Error

CFL : Courant-Friedrichs-Lewy

2. Preliminaries

Definition 1 *[33] The Riemann–Liouville fractional integral of order $\alpha > 0$ is defined by*

$$J^{\alpha}\mathrm{f(t)} = \frac{1}{\Gamma(\alpha)} \int_0^t (t-\tau)^{(\alpha-1)}\mathrm{f}(\tau)\mathrm{d}\tau$$

Where $\Gamma(\alpha)$ denotes the Gamma function, a continuous extension of the factorial to real and complex numbers. This operator generalizes the classical notion of integration and provides the groundwork for defining fractional-order derivatives.

inition 2 *[20] The Riemann–Liouville fractional derivative of a function $f(t)$, for a*

Received: August 05, 2025

International Journal of Applied Mathematics

Volume 38 No. 12s, 2025

ISSN: 1311-1728 (printed version); ISSN: 1314-8060 (on-line version)

fractional order a>0, is defined as

$$D^{\alpha}\mathrm{f(t)} = \frac{d^m}{dt^m}\left(\frac{1}{\Gamma(m-\alpha)}\int_0^t \frac{\mathrm{f}(\tau)}{(t-\tau)^{(\alpha+1-m)}}\,\mathrm{d}\tau\right),$$

Where m = ⌈α⌉ represents the smallest integer not less than α. In the special case where α

is an integer, that is α = m, the formula reduces to the classical m^{th} order derivative:

$$D^{\alpha}\mathrm{f(t)} = \frac{d^m}{dt^m}\,\mathrm{f}(\tau).$$

Definition 3 *[34] The Caputo fractional derivative of a function f(t), for an order α > is defined as*

$$D_*^{\alpha} f(t) = J^{m-\alpha} D^m f(t),$$

Where m is the smallest integer such that m-1 < a ≤m. This definition can be written explicitly as

$$D_*^{\alpha} f(t = \begin{cases} \frac{1}{\Gamma(m-\alpha)}\int_0^t \frac{\mathrm{f}^m(\tau)}{(t-\tau)^{(\alpha+1-m)}}\,\mathrm{d}\tau, & if\ m-1<\alpha<m \\ \frac{d^m}{dt^m}\,\mathrm{f}(t), & \alpha = m. \end{cases}$$

Definition 4 *[21] In fractional calculus, the Laplace transform of the fractional derivative of order α > 0 is expressed as*

$$\mathcal{L}\{D^{\alpha}f(t)\}(s) = s^{\alpha}\,\mathcal{L}\,\{f(t)\,(s) - \sum_{k=0}^{m-1} s^{\alpha-k-1}\,f^{(k)}(0).$$

Where m = ⌈α⌉ denotes the smallest integer not less than α. For the fractional integral of order α, the Laplace transform takes the form

$$\mathcal{L}\{J^{\alpha}f(t)\}(s) = \frac{\mathcal{L}\{f\,(t)\}(\mathrm{s})}{s^{\alpha}}$$

These Laplace transform rules allow fractional differential equations to be transformed into algebraic equations in the s-domain, facilitating their analysis and solution.

Definition 5 *[34] The Mittag-Leffler function is defined as $E_{\alpha,\beta}(z) = \sum_{n=0}^{\infty}\frac{z^n}{\Gamma(\alpha n+\beta)}$,*

α and β are parameters. Its inverse function $E^{-1}{}_{\alpha,\beta}(w)$ satisfies $E_{\alpha,\beta}(z) = w$,

Received: August 05, 2025

International Journal of Applied Mathematics

Volume 38 No. 12s, 2025

ISSN: 1311-1728 (printed version); ISSN: 1314-8060 (on-line version)

but is typically evaluated numerically due to the absence of a closed-form expression.

3. Mathematical Description

The three dimensional time fractional advection diffusion equation for the domain

$\Omega = [0, L_x]\times[0, L_y]\times[0, L_z]$

$$\frac{\partial^\alpha C}{\partial t^\alpha} = \mathrm{D}\left(\frac{\partial^2 C}{\partial x^2} + \frac{\partial^2 C}{\partial y^2} + \frac{\partial^2 C}{\partial z^2}\right) - \mathrm{u_x}\frac{\partial C}{\partial x} - \mathrm{u_y}\frac{\partial C}{\partial y} - \mathrm{u_z}\frac{\partial C}{\partial z} - \mathrm{QC} - \lambda C. \quad (1)$$

Where, $C = C(x, y, z, t)$ be the concentration field. The initial and boundary conditions for the three- dimensional case are as follows: $C(x, y, z, 0) = f(x, y, z)$;

$C(0, y, z, t)=C(L_x, y, z, t)=0, C(x, 0, z, t)=C(x, L_y, z, t)=0, C(x, y, 0, t)=C(x, y, L_z, t)=0.$

The pollutant concentration $C(x, y, z)$ varies with spatial coordinates x, y, z and time t. The fractional time derivative α $(0 < \alpha \leq 1)$ captures memory effects in diffusion. The velocity components u_x, u_y, and u_z in the x-, y-, and z-directions are constants. The diffusion coefficient is D, the pollutant source term is Q, and the decay term is λC. For simplicity, the source term is taken as $Q(C) = 0$

$$C(x, y, z, t) = \sum_{n=1}^{\infty}\sum_{m=1}^{\infty}\sum_{p=1}^{\infty} X_n(x)Y_m(y)Z_p(z)T_{m.n.p}(t) \quad (2)$$

From the equations (1) and (2)

$$\sum_{n=1}^{\infty}\sum_{m=1}^{\infty}\sum_{p=1}^{\infty} X_n(x)Y_m(y)Z_p(z)\frac{\partial^\alpha T_{m.n.p}(t)}{\partial t^\alpha}$$

$$= \sum_{n=1}^{\infty}\sum_{m=1}^{\infty}\sum_{p=1}^{\infty} D\left(X''_n(x)Y_m(y)Z_p(z)T(t) + X_n(x)Y''_m(y)Z_p(z)T(t) - \lambda\right)$$

Separating variables,

$$\frac{1}{T}.\frac{\partial^\alpha T_{m.n.p}(t)}{\partial t^\alpha} = \mathrm{D}\left[\frac{X_n''(x)}{X_n(x)} + \frac{Y_m''(y)}{Y_m(y)} + \frac{Z_p''(z)}{Z_p(z)}\right] - \left[u_x\frac{X_n'(x)}{X_n(x)} + u_y\frac{Y_m'(y)}{Y_m(y)} + u_z\frac{Z_p'(z)}{Z_p(z)}\right] - \lambda$$

$$\frac{1}{T}.\frac{\partial^\alpha T_{m.n.p}(t)}{\partial t^\alpha} + \lambda = \mathrm{D}\left[\frac{X_n''(x)}{X_n(x)} + \frac{Y_m''(y)}{Y_m(y)} + \frac{Z_p''(z)}{Z_p(z)}\right] - \left[u_x\frac{X_n'(x)}{X_n(x)} + u_y\frac{Y_m'(y)}{Y_m(y)} + u_z\frac{Z_p'(z)}{Z_p(z)}\right] = -\gamma,$$

Received: August 05, 2025

International Journal of Applied Mathematics

Volume 38 No. 12s, 2025

ISSN: 1311-1728 (printed version); ISSN: 1314-8060 (on-line version)

where γ is the separation constant. The time-dependent term depends only on t, while the spatial terms depend separately on x, y, and z. For the equality to hold for all variables, both sides must equal the same constant, denoted by $-\gamma$. Since each spatial term is a function of a single variable, they are set equal to constants $-k_x^2$, $-k_y^2$, and $-k_z^2$, satisfying $\gamma = k_x^2 + k_y^2 + k_z^2$. This separation reduces the original equation into one time-fractional ordinary differential equation and three spatial ordinary differential equations.

$$\frac{\partial^{\alpha} T_{m.n.p}(t)}{\partial t^{\alpha}} + (\lambda + \gamma)\, T_{m.n.p}(t) = 0. \tag{3}$$

$$DX_n'' - u_x X_n' + k_x^2 X_n = 0, \tag{4}$$

$$DY_m'' - u_y Y_m' + k_y^2 Y_m = 0, \tag{5}$$

$$DZ_p'' - u_z Z_p' + k_z^2 Z_p = 0, \tag{6}$$

From (4) $X_n(x) = \exp\left(\frac{\mu_x x}{2D}\right)(A\cos(\mu_x x) + B\sin(\mu_x x))$ with $\mu_x^2 = k_x^2 - \frac{k_x^2}{2D}$.

Applying boundary Conditions, $X(0) = X(L_x) = 0$; $X_n(0) \neq 0$

$$\Rightarrow \quad X_n(x) = B\exp\left(\frac{\mu_x x}{2D}\right)\sin(\mu_x x)$$

$$X(L_x) = 0 \Rightarrow \quad B\exp\left(\frac{\mu_x x}{2D}\right)\sin(\mu_x x) = 0 \quad \Rightarrow \quad \sin(\mu_x Lx) = 0$$

$$\Rightarrow \quad \mu_x = \frac{n\pi}{Lx}, \quad n \in N.$$

$$\text{Thus, } X_n(x) = \exp\left(\frac{\mu_x x}{2D}\right)\sin\left(\frac{n\pi x}{Lx}\right), \tag{7}$$

$$k_x^2 = \mu_x^2 + \left(\frac{\mu_x x}{2D}\right)^2 \Rightarrow \quad k_x^2 = \left(\frac{n\pi}{Lx}\right)^2 + \left(\frac{\mu_x}{2D}\right)^2,$$

$$\text{Similarly,} \quad Y_m(Y) = \exp\left(\frac{\mu_y y}{2D}\right)\sin\left(\frac{m\pi y}{Ly}\right) \tag{8}$$

$$Z_p(z) = \exp\left(\frac{\mu_z z}{2D}\right)\sin\left(\frac{p\pi z}{Lz}\right), \tag{9}$$

$$\text{with } k_y^2 = \left(\frac{n\pi}{Ly}\right)^2 + \left(\frac{\mu_y}{2D}\right)^2; \; k_z^2 = \left(\frac{n\pi}{Lz}\right)^2 + \left(\frac{\mu_z}{2D}\right)^2.$$

From the equation (3)

$$\frac{\partial^{\alpha} T_{m.n.p}(t)}{\partial t^{\alpha}} + (\lambda + \gamma)\, T_{m.n.p}(t) =, \tag{10}$$

Received: August 05, 2025

International Journal of Applied Mathematics

Volume 38 No. 12s, 2025

ISSN: 1311-1728 (printed version); ISSN: 1314-8060 (on-line version)

$$ {}_0^cD_t^{\alpha} T_{m.n.p}(t) + (\lambda + \gamma)\, T_{m.n.p}(t) = 0, \qquad (11) $$

Applying Laplace Transform,

$$ \mathcal{L}[{}_0^cD_t^{\alpha} T_{m.n.p}(t)] + \mathcal{L}[(\lambda + \gamma)\, T_{m.n.p}(t)] = \mathcal{L}[0], $$

where $\widetilde{T}_{m.n.p}(s)$ is the Laplace transform of $T_{m.n.p}(t)$.

$$ \Longrightarrow \{s^{\alpha}\widetilde{T}_{m.n.p}(s) - \sum_{k=0}^{n-1} s^{(\alpha-k-1)}\, T_{m,n,p}{}^{(k)}(0)\} + \lambda_{n,m,p}\widetilde{T}_{m.n.p}(s) = 0, $$

This gives, $s^{\alpha}\widetilde{T}_{m.n.p}(s) - \sum_{k=0}^{0} s^{(\alpha-1)}\, T_{m,n,p}{}^{(k)}(0)\} + (\lambda_{n,m,p} + s)\, \widetilde{T}_{m.n.p}(s) = 0$,

Or, $\widetilde{T}_{m.n.p}(s) = \frac{s^{(\alpha-1)} T_{m,n,p}(0)}{\{s^{\alpha} + (\lambda + \gamma)\}}$. Applying inverse Laplace transform,

$$ T_{m.n.p}(s) = T_{m.n.p}(0)\mathcal{L}^{-1}\left(\frac{s^{\alpha-\beta}}{s^{\alpha-\theta}}\right) = x^{\beta-1}E_{\alpha,\beta}(\theta x^{\alpha}) \Longrightarrow \beta = 1,\ \theta = -\lambda - \gamma. $$

$T_{m.n.p}(t) = T_{m.n.p}(0)t^{(\alpha-1)}E_{\alpha,\beta}(-\lambda - \gamma)t^{\alpha}$, Here, $E_{\alpha,1}$ denotes the Mittag-Leffler function.

The constant $T_{n,m,p}$ (0) is determined by the initial condition and $\phi(x, y, z) = \frac{u_x x + u_y y + u_z z}{2D}$.

Therefore, equation (2) can be expressed as

$$ C(x, y, z, t) = \sum_{n=1}^{\infty}\sum_{m=1}^{\infty}\sum_{p=1}^{\infty} A_{n,m.p}\, exp(\phi(x, y, z)) \sin\left(\frac{n\pi x}{Lx}\right) \sin\left(\frac{m\pi y}{Ly}\right) \sin\left(\frac{p\pi z}{Lz}\right). $$

$E_{\alpha,1}(-(\lambda + \gamma_{n,m,p})t^{\alpha})$. Where, $\gamma_{n,m,p} = D\left(\left(\frac{n\pi}{Lx}\right)^2 + \left(\frac{m\pi}{Ly}\right)^2 + \left(\frac{p\pi}{Lz}\right)^2 + \frac{u_x x + u_y y + u_z z}{4D^2}\right)$ and $A_{n,m.p}$ (t) are the Fourier coefficients determined by the initial condition, determining coefficient $A_{n,m,p;}$ using the condition C(x, y, z, 0) = f(x, y, z);

$$ f(x, y, z) = \sum_{n=1}^{\infty}\sum_{m=1}^{\infty}\sum_{p=1}^{\infty} A_{n,m.p}\, exp(\phi(x, y, z)) \sin\left(\frac{n\pi x}{Lx}\right) \sin\left(\frac{m\pi y}{Ly}\right) \sin\left(\frac{p\pi z}{Lz}\right). $$

The Fourier coefficients $A_{n,m,p}$ (0) are determined by applying the initial condition C(x, y, z, 0) = f(x, y, z) and utilizing the orthogonally property of sine functions $A_{n,m.p}(0) = \frac{8}{Lx\, Ly\, Lz}\int_0^{Lx}\int_0^{Ly}\int_0^{Lz} f(x, y, z) \exp(-\phi(x, y, z)) \sin\left(\frac{n\pi x}{Lx}\right) \sin\left(\frac{m\pi y}{Ly}\right) \sin\left(\frac{p\pi z}{Lz}\right) dz\, dy\, dx.$

The analytical solution is obtained by applying the separation of variables, breaking the problem down into spatial and temporal parts. Spatial solutions consist of exponential and sine functions that satisfy boundary conditions and incorporate advection effects. The temporal component is a fractional differential equation solved using Laplace transform techniques, resulting in a Mittag-Leffler function that models anomalous diffusion behavior. The eigenvalues of each spatial dimension combine into a separation constant, while Fourier coefficients are calculated by a projection of the orthogonal projection of

International Journal of Applied Mathematics

Volume 38 No. 12s, 2025

ISSN: 1311-1728 (printed version); ISSN: 1314-8060 (on-line version)

the initial condition. This approach provides an exact, closed-form solution useful for benchmarking numerical methods and exploring how parameters such as flow velocity and fractional order influence dispersion. The solution effectively captures asymmetric advection, memory effects, and non-standard diffusion patterns relevant to environmental and biological transport processes.

4. Plots of Pollution Dispersion at various Orders Using Analytical Solution

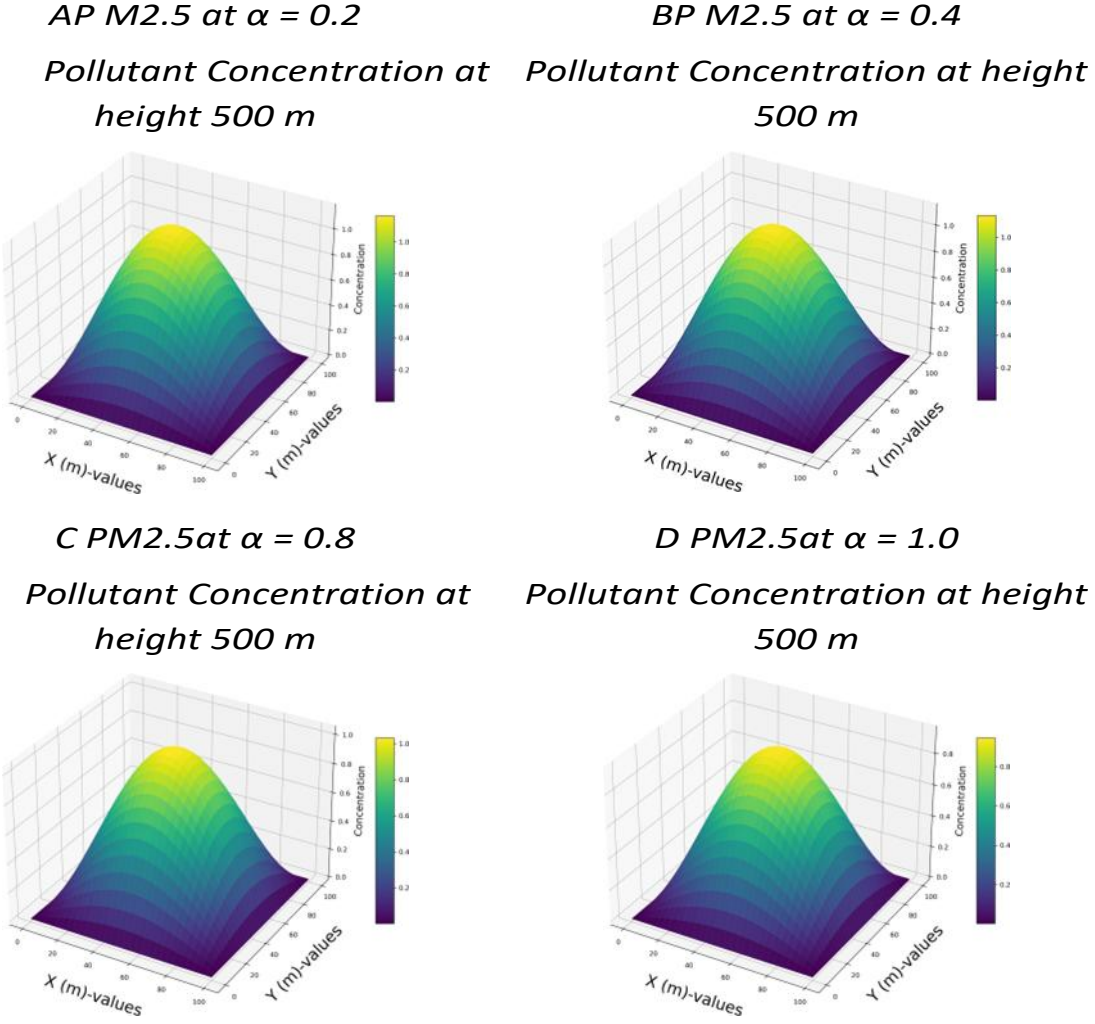

Figure 1: Three Dimensional Plot of PM2.5 with D = 10, AP M2.5 at α = 0.2,
BP M2.5 at α = 0.4, CP M2.5 at α = 0.8, DP M2.5 at α = 1.0.

Figure 1 illustrates the pollutant distribution over the horizontal *x–y* plane at a vertical level at height of

Received: August 05, 2025

International Journal of Applied Mathematics

Volume 38 No. 12s, 2025

ISSN: 1311-1728 (printed version); ISSN: 1314-8060 (on-line version)

500 meters, as derived from the analytical solution of a three-dimensional time-fractional advection-diffusion equation (FADE) with fractional order $\alpha = 0.4$. The simulated domain covers 100m × 100m laterally and rises up to 1500m in altitude. A uniform advection speed of 0.1m/h is assumed in all spatial directions, along with a diffusion coefficient set to $D = 10$. The initial condition adopts a trigonometric function that aligns with the boundary constraints, simulating a localized emission point. Time-dependent behavior is modeled through the Mittag-Leffler function to reflect the memory effects inherent in fractional-order transport. At a representative location ($0.2L_x$, $0.3L_y$, 500, m), the pollutant level at $t = 12$ hours is approximately 5.618×10^{-1} for $\alpha = 0.4$. Varying the fractional order reveals a notable decline in concentration: from 5.804×10^{-1} for $\alpha = 0.2$ down to 4.961×10^{-1} for $\alpha = 0.8$, and further to 4.430×10^{-1} in the classical diffusion case ($\alpha = 1.0$). This trend confirms that lower α values correspond to stronger memory effects, resulting

in slower dispersion and prolonged pollutant presence. The roughly 24% drop in concentration between $\alpha = 0.2$ and $\alpha = 1.0$ highlights the critical role of anomalous transport. Moreover, intermediate α values (e.g., $\alpha = 0.4$) yield persistent concentration gradients and non-Gaussian plume profiles, reflecting time- varying diffusivity and complex transport pathways. These results underscore the need to include fractional dynamics in models dealing with environmental transport, particularly in heterogeneous or turbulent systems. The result for $\alpha = 0.4$ at 12 hours provides a key reference point for comparison with observed data. Overall, fractional modeling indicates that pollutant removal times may be extended by 30-50% in subdiffusive conditions, suggesting regulatory policies should integrate such models for more reliable assessment and management strategies.

5. Numerical Simulation of Three-Dimensional FADE

5.1 Numerical Simulation

The 3D-TFAD for the domain $\Omega = [0, L_x] \times [0, L_y] \times [0, L_z]$ is given by:

$$\frac{\partial^{\alpha} \mathrm{C}(x_m,\ y_l, z_{p,\ t^n})}{\partial t^{\alpha}} = \mathrm{D}\left(\frac{\partial^2 \mathrm{C}(x_m,\ y_l, z_{p,\ t^n})}{\partial x^2} + \frac{\partial^2 \mathrm{C}(x_m,\ y_l, z_{p,\ t^n})}{\partial y^2} + \frac{\partial^2 \mathrm{C}(x_m,\ y_l, z_{p,\ t^n})}{\partial z^2}\right)$$
$$- \mathrm{u_x} \frac{\partial \mathrm{C}(x_m,\ y_l, z_{p,\ t^n})}{\partial x} - \mathrm{u_y} \frac{\partial \mathrm{C}(x_m,\ y_l, z_{p,\ t^n})}{\partial y} - \mathrm{u_z} \frac{\partial \mathrm{C}(x_m,\ y_l, z_p, t^n)}{\partial z}$$
$$- \mathrm{Q}\ \mathrm{C}(x_m,\ \ y_l,\ z_{p,\ t^n}) - \lambda\, \mathrm{C}(x_m,\ \ y_l,\ z_{p,\ t^n}). \qquad (12)$$

The initial and boundary conditions for the three-dimensional case are as follows: $C(x, y, z, 0) = f(x, y, z)$, $C(0, y, z, t) = C(L_x, y, z, t) = 0$, $C(x, 0, z, t) = C(x, L_y, z, t) = 0$, $C(x, y, 0, t) = C(x, y, L_z, t) = 0$.

To approximate the Caputo fractional time derivative of order α ($0 < \alpha \leq 1$) within a three-dimensional domain, the Grünwald–Letnikov discretization is applied using a

Received: August 05, 2025

International Journal of Applied Mathematics

Volume 38 No. 12s, 2025

ISSN: 1311-1728 (printed version); ISSN: 1314-8060 (on-line version)

time step of size k. This approach is well-suited for initial value problems in multidimensional spaces. The Caputo fractional derivative can be expressed in an approximate form as:

$$\frac{\partial^{\alpha} \mathrm{C}(x_m,\ y_l, z_{p,\ t^n})}{\partial t^{\alpha}} = \frac{1}{\Gamma(1-\alpha)} \sum_{j=0}^{n} w_j \binom{\alpha}{j} \mathrm{C}(x_m,\quad y_l,\ z_{p,} t^{n-j}). \tag{13}$$

Here, $C(x_m, y_l, z_p, t^n)$ represents the concentration at spatial coordinates (x_m, y_l, z_p) and time t^n. Here, the weights w_j are derived as:

$$W_j = \frac{(-1)^j \Gamma(1+\alpha)}{\Gamma(j+1)\,\Gamma(\alpha-j+1)}.$$

For non-integer orders of α, these weights stem from the binomial coefficient. The summation must be changed in the following ways in order to apply the caputo definition

$$\frac{\partial^{\alpha} \mathrm{C}(x_m,\ y_l, z_{p,\ t^n})}{\partial t^{\alpha}} = \frac{1}{\Gamma(2-\alpha)} \sum_{j=0}^{n} \binom{n-j+\alpha-1}{n-j} \frac{\mathrm{C}(x_m,\ y_l, z_{p,} t^{j}) - \mathrm{C}(x_m,\ y_l, z_{p,} t^{j-1})}{k^{\alpha}},$$

$$\text{with } \sum_{j=0}^{n}{}^{n} \binom{n-j+\alpha-1}{n-j} = \frac{\Gamma(n-j+\alpha)}{\Gamma(\alpha)\Gamma(n-j-1)}.$$

Spatial derivatives are approximated using central finite differences as follows:

$$\frac{\partial^2 \mathrm{C}(x_m,\quad y_l,\ z_{p,} t^n)}{\partial x^2} = \frac{\mathrm{C}(x_{m+1},\quad y_l,\ z_{p,} t^n) - 2\mathrm{C}(x_m,\quad y_l,\ z_{p,} t^n) + \mathrm{C}(x_{m-1},\quad y_l,\ z_{p,} t^n)}{h_x^2}$$

$$\frac{\partial^2 \mathrm{C}(x_m,\quad y_l,\ z_{p,} t^n)}{\partial y^2} = \frac{\mathrm{C}(x_m,\quad y_{l+1},\ z_{p,} t^n) - 2\mathrm{C}(x_m,\quad y_l,\ z_{p,} t^n) + \mathrm{C}(x_{m-1},\quad y_{l-1},\ z_{p,} t^n)}{h_y^2}$$

$$\frac{\partial^2 \mathrm{C}(x_m,\quad y_l,\ z_{p,}\ t^n)}{\partial z^2} = \frac{\mathrm{C}(x_m,\quad y_l,\ z_{p+1,}\ t^n) - 2\mathrm{C}(x_m,\ y_l,\ z_{p,} t^n) + \mathrm{C}(x_m,\ y_l,\ z_{p-1,} t^n)}{h_z^2}$$

$$\nabla^2 \mathrm{C}(x_m, y_l,\ z_{p,}\ t^n) = \frac{\mathrm{C}(x_{m+1},\ y_l, z_{p,} t^n) - 2\mathrm{C}(x_m,\ y_l, z_{p,} t^n) + \mathrm{C}(x_{m-1},\ y_l, z_{p,} t^n)}{h_x^2}$$

$$+ \frac{\mathrm{C}(x_m,\ y_{l+1}, z_{p,} t^n) - 2\mathrm{C}(x_m,\ y_l, z_{p,} t^n) + \mathrm{C}(x_{m-1},\ y_{l-1}, z_{p,} t^n)}{h_y^2}$$

$$+ \frac{\mathrm{C}(x_m,\quad y_l,\ z_{p+1,}\ t^n) - 2\mathrm{C}(x_m,\ y_l,\ z_{p,} t^n) + \mathrm{C}(x_m,\ y_l,\ z_{p-1,} t^n)}{h_z^2}$$

Here, h_x, h_y and h_z are the spatial step sizes along the x, y, and z directions, respectively.

For $x-$ direction:

$$\frac{\partial \mathrm{C}(x_m,\quad y_l,\ z_{p,} t^n)}{\partial \mathrm{x}} = \frac{\mathrm{C}(x_{m+1},\quad y_l,\ z_{p,} t^n) - \mathrm{C}(x_{m-1},\quad y_l,\ z_{p,} t^n)}{2h_x}$$

Received: August 05, 2025

International Journal of Applied Mathematics

Volume 38 No. 12s, 2025

ISSN: 1311-1728 (printed version); ISSN: 1314-8060 (on-line version)

For $y-$ direction:

$$\frac{\partial \mathrm{C}(x_m,\ \ y_l,\ z_{p,}t^n)}{\partial \mathrm{y}} = \frac{\mathrm{C}\left(x_m,\ \ y_{l+1},\ z_{p,}t^n\right) - \mathrm{C}\left(x_m,\ \ y_{l-1},\ z_{p,}t^n\right)}{2h_y}$$

For $z-$ direction:

$$\frac{\partial \mathrm{C}(x_m,\ \ y_l,\ z_{p,}t^n)}{\partial \mathrm{z}} = \frac{\mathrm{C}\left(x_m,\ \ y_l,\ z_{p+1,}t^n\right) - \mathrm{C}\left(x_m,\ \ y_1,\ z_{p-1,}t^n\right)}{2h_z}$$

The total advection term in three dimensions is given by the sum of these components.

$$\nabla.\,\mathrm{C} = \frac{\mathrm{C}(x_{m+1},\ y_l, z_{p,}t^n) - \mathrm{C}(x_{m-1},\ y_l, z_{p,}t^n)}{2h_x} + \frac{\mathrm{C}(x_m,\ y_{l+1}, z_{p,}t^n) - \mathrm{C}(x_m,\ y_{l-1}, z_{p,}t^n)}{2h_y}$$

(15)

Equation (12) reduces

$$\frac{1}{\Gamma(2-\alpha)} \sum_{j=0}^{n} \binom{n-j+\alpha-1}{n-j} \frac{\mathrm{C}(x_m,\ y_l, z_{p,}t^j) - \mathrm{C}(x_m,\ y_l, z_{p,}t^{j-1})}{k^\alpha}$$

$$= \mathrm{D}\left[\begin{array}{l} \frac{\mathrm{C}(x_{m+1},\ y_l, z_{p,}t^n) - 2\mathrm{C}(x_m,\ y_l, z_{p,}t^n) + \mathrm{C}(x_{m-1},\ y_l, z_{p,}t^n)}{h_x^2} \\ + \frac{\mathrm{C}(x_m,\ y_{l+1}, z_{p,}t^n) - 2\mathrm{C}(x_m,\ y_l, z_{p,}t^n) + \mathrm{C}(x_{m-1},\ y_{l-1}, z_{p,}t^n)}{h_y^2} \\ + \frac{\mathrm{C}(x_m,\ y_l, z_{p+1,}\,t^n) - 2\mathrm{C}(x_m, y_l, z_{p,}t^n) + \mathrm{C}(x_m, y_l, z_{p-1,}t^n)}{h_z^2} \end{array}\right]$$

$$- u_x \frac{\mathrm{C}(x_{m+1},\ y_l, z_{p,}t^n) - \mathrm{C}(x_{m-1},\ y_l, z_{p,}t^n)}{2h_x} - u_y \frac{\mathrm{C}(x_m,\ y_{l+1}, z_{p,}t^n) - \mathrm{C}(x_m,\ y_{l-1}, z_{p,}t^n)}{2h_y}$$

$$- u_z \frac{\mathrm{C}(x_m,\ y_l, z_{p+1,}t^n) - \mathrm{C}(x_m,\ y_1, z_{p-1,}t^n)}{2h_z} - \mathrm{Q_{m,\,l,\,p}} - \lambda\,\mathrm{C}(x_m,\ \ y_l,\ z_{p,}t^n). \qquad (16)$$

Using $V_{m,l,p}^{n+1} = \mathrm{C}\left(x_m,\ \ y_{l+1},\ z_{p,}t^{n+1}\right)$), we account for the source term Q and approximate the concentration at the next time step. The discretized equation for three-dimensional fractional partial differential equations with a source term is:

$$\frac{1}{\Gamma(2-\alpha)} \sum_{j=0}^{n} \binom{n-j+\alpha-1}{n-j} \frac{V_{m,l,p}^{j} - V_{m,l,p}^{j-1}}{k^\alpha}$$

$$= \mathrm{D}\left[\frac{V_{m+1,l,p}^{n} - 2V_{m,l,p}^{n} + V_{m-1,l,p}^{n}}{h_x^2} + \frac{V_{m,l+1,p}^{n} - 2V_{m,l,p}^{n} + V_{m,l-1,p}^{n}}{h_y^2} + \frac{V_{m,l,p+1}^{n} - 2V_{m,l,p}^{n} + V_{m,l,p-1}^{n}}{h_y^2}\right]$$

$$- u_x \frac{V_{m+1,l,p}^{n} - V_{m-1,l,p}^{n}}{2h_x} - u_y \frac{V_{m,l+1,p}^{n} - V_{m,l-1,p}^{n}}{2h_y} - u_z \frac{V_{m,l,p+1}^{n} - V_{m,l,p-1}^{n}}{2h_z} + \mathrm{Q_{m,l,p}} - \lambda\, V_{m,l,p}^{n}.$$

Where, Q is the source term (positive for sources, negative for sinks) at the grid point (x_m, y_l, z_p). Other parameters remain as previously defined, D: diffusion coefficient, u_x, u_y, u_z: velocity components, α: fractional order of the time derivative, $\Gamma(2-\alpha)$: Gamma function for the fractional term, λ: reaction rate coefficient. Thus we have

Received: August 05, 2025

International Journal of Applied Mathematics

Volume 38 No. 12s, 2025

ISSN: 1311-1728 (printed version); ISSN: 1314-8060 (on-line version)

$$V_{m,l,p}^{n+1} = V_{m,l,p}^{n} + a_1\left[D\left(\frac{V_{m+1,l,p}^{n}-2V_{m,l,p}^{n}+V_{m-1,l,p}^{n}}{h_x^2} + \frac{V_{m,l+1,p}^{n}-2V_{m,l,p}^{n}+V_{m,l-1,p}^{n}}{h_y^2} + \frac{V_{m,l,p+1}^{n}-2V_{m,l,p}^{n}+V_{m,l,p-1}^{n}}{h_y^2}\right) - \beta_x \frac{V_{m+1,l,p}^{n}-V_{m-1,l,p}^{n}}{2h_x} - \beta_y \frac{V_{m,l+1,p}^{n}-V_{m,l-1,p}^{n}}{2h_y} - \beta_z \frac{V_{m,l,p+1}^{n}-V_{m,l,p-1}^{n}}{2h_z}\right]$$

$$- (1-a_1)\left[\frac{1}{\Gamma(2-\alpha)}\sum_{j=0}^{n}\binom{n-j+\alpha-1}{n-j}\frac{V_{m,l,p}^{j}-V_{m,l,p}^{j-1}}{k^{\alpha}}\right] + KQ_{m,l,p} - k\lambda V_{m,l,p}^{n}. \qquad [17]$$

5.2 Consistency, Stability and Convergence

The consistency, stability, and convergence characteristics of the implicit finite difference scheme are rigorously examined, wherein, as indicated by (16), the scheme incurs a local truncation error denoted by R_j^n.

Consistency: The numerical scheme for the three-dimensional FADE maintains consistency with the continuous equation, achieving a local truncation error (LTE) that vanishes as k, h_x, h_y, $h_z \to 0$. The Caputo fractional derivative is discretized via the Grünwald-Letnikov method, as in (13), with an error of $O(k^{2-\alpha})$ for $0 < \alpha \leq 1$. Diffusion terms are approximated using central differences, as shown in (14), leading to an error of

$O(h^2_x + h^2_y + h^2_z)$. Similarly, advection terms discretized by (15) yield the same error order. The source term Q and reaction term $-\lambda C$ are evaluated exactly at grid points (m, l, p) and discrete time t^n, introducing no additional error. At these points, the truncation error is O(1), reflecting precise computation. Overall Consistency: The total LTE is: $LTE = O(k^{2-\alpha}) + O(h_x^2) + O(h^2_y) + O(h^2_z)$. As k, h_x, h_y, $h_z \to 0$, the scheme remains consistent. For $\alpha \to 1$, the formulation converges to the classical advection-diffusion.

Stability: The stability of the numerical scheme is analyzed using the von Neumann method under Dirichlet boundary conditions. For the homogeneous case ($Q = 0$, $\lambda = 0$), the solution is represented as a Fourier mode, $V_{m,l,p}^{n} = \xi^n e^{i(m\theta_x + l\theta_y + p\theta_z)}$, with stability requiring the amplification factor ξ to satisfy $|\xi| \leq 1$. Spatial discretization terms are defined for diffusion (D_x, D_y, D_z) and advection (A_x, A_y, A_z) such that

$A_x \sim \frac{u_x}{h_x}\left(V_{l+1,m,p}^{n} - V_{l,m,p}^{n}\right)$, $A_y \sim \frac{u_y}{h_y}\left(V_{l,m+1,p}^{n} - V_{l,m,p}^{n}\right)$ and $A_z \sim \frac{u_z}{h_z}\left(V_{l,m,p+1}^{n} - V_{l,m,p}^{n}\right)$.

with the total operator $\mathcal{L}$ incorporating these contributions. The amplification equations becomes $\xi = 1 + a_1\mathcal{L} + (1 + a_1)\frac{(1-\xi^{-1})^{1-\alpha}}{\Gamma(2-\alpha)k^{\alpha}}$. For $a_1 = 1$(explicit advection-diffusion),Dirichlet boundary conditions impose stability constraints such that

Received: August 05, 2025

International Journal of Applied Mathematics

Volume 38 No. 12s, 2025

ISSN: 1311-1728 (printed version); ISSN: 1314-8060 (on-line version)

$k \leq \min\left(\frac{h^2{}_x}{2D}, \frac{h^2{}_y}{2D}, \frac{h^2{}_z}{2D}, \frac{h_x}{|u_x|}, \frac{h_y}{|u_y|}, \frac{h_z}{|u_z|}\right)$. For $a_1 = 0$ (explicit fractional term), stability is satisfied if $k^{\alpha} \leq \Gamma(2-\alpha)\, C(\alpha)$. The scheme is unstable for $a_1 < 1$ due to explicit fractional handling, whereas conditional stability is ensured for $a_1 = 1$, subject to CFL and diffusion conditions. Implicit treatment of the fractional derivative is recommended for improved stability under Dirichlet boundaries.

Convergence: To prove the convergence of the three-dimensional numerical solution,

let $C(x_l, y_m, z_p, t_n)$ be the exact solution at the mesh point (x_l, y_m, z_p, t_n) and $C^n_{l,m,p}$ be

the numerical solution. Define the error as $e^n_{l,m,p} = C(x_l, y_m, z_p, t_n) - C^n_{l,m,p}$, where l, m, p index the spatial grid in x, y, and z, respectively, and n represents the time step. The numerical scheme results in the error equation

$$L_1 e^n_{l,m,p} = L_2 e^{n-1}_{l,m,p} + R^n_{l,m,p}.$$

Where L_1 and L_2 are numerical operators, and $R^n{}_{l,m,p}$ is the local truncation error(LTE).Taking the L^{∞} norm of the error, extended to three spatial dimensions, gives: $\|e^n\|_{\infty} = \max_{l,m,n} |e^n_{l,m.n}|$. Using the error equations, the norm of the error satisfies: $\|e^n\|_{\infty} \leq \|L_2 e^{n-1}\|_{\infty} + \|R^n\|_{\infty}$. For a stable numerical scheme, it is assumed that $\|L_2 e^{n-1}\|_{\infty} \leq \|e^{n-1}\|_{\infty}$. The local truncation error for a

Three-dimensional scheme scales as $R^n_{l,m,p} = O(\Delta t^{(2-\alpha)}) + O(\Delta x^2) + O(\Delta y^2) + O(\Delta z^2)$, where Δx, Δy, Δz are the spatial step sizes, and Δt is The temporal step size. If the spatial grid is uniform ($\Delta x = \Delta y = \Delta z = h$), the truncation error simplifies to: $R_n{}^{l,m,p} = O(\Delta t^{(2-\alpha)}) + O(h^2)$. Thus, the maximum truncation error is bounded as: $\|R_n\|_{\infty} \leq C\_R\ (\Delta t^{(2-\alpha)} + h^2)$, where C_R is a constant. Using this in the error equation, we obtain: $\|e_n\|_{\infty} \leq \|e_{n-1}\|_{\infty} + R_{max} \leq \ldots \leq \|e^0\|_{\infty} + R_{max.}$

By recursion, this yields:

$\|e_n\|_{\infty} \leq \|e^{n-1}\|_{\infty} + R_{max} \leq \|e_{n-2}\|_{\infty} + 2R_{max} \leq \cdots \leq \|e_0\|_{\infty} + n\ R_{max}$. Since the initial error is zero $(e^0_{l,m,} = 0)$ it follows that: $\|e^n\|_{\infty} \leq n\ R_{max}$. For $n = T/\Delta t$, substituting R_{max}, we have: $\|e^n\|_{\infty} \leq (T/\Delta t)\ C_R\ (\Delta t^{(2-\alpha)} + h^2)$. Simplifying, this becomes: $\|e^n\|_{\infty} \leq T\ C\_R\ \Delta t^{(1-\alpha)} + (T\ h^2)/\Delta t$. To ensure convergence as $\Delta t, h \to 0$, the temporal and spatial errors should balance, i.e.,$h^2/\Delta t = O(\Delta t^{(1-\alpha)})$. By choosing h and Δt accordingly, both terms vanish as the grid is refined, proving that:$\|e^n\|_{\infty} \to 0$ as $\Delta t, h \to 0$. At the boundaries of the region, Dirichlet boundary conditions are imposed for the one-dimensional case, ensuring the pollutant concentration remains zero at both spatial endpoints for any time t, expressed as $C(0, t) = C(L_x, t) = 0$, and similarly for higher dimensions $C(0, t) = C(L_y, t) = 0$, $C(0, t) = C(L_z, t) = 0$. The pollutant concentration at the boundaries of the domain is maintained at zero, signifying no pollutant escapes the region. Non reflective boundary conditions are

Received: August 05, 2025

International Journal of Applied Mathematics
Volume 38 No. 12s, 2025
ISSN: 1311-1728 (printed version); ISSN: 1314-8060 (on-line version)

applied, ensuring the pollutant does not re-enter the domain from opposing boundaries. Initially, the pollutant is localized at the center of the domain. In the one-dimensional case, the pollutant concentration is set to 1 within the central region of the spatial domain, specifically between 0 and L_x, at the initial time, while being zero elsewhere. For two-dimensional and three-dimensional cases, the pollutant is similarly localized in the central part of the domain. Along the y-axis, the concentration is 1 within $0 < y < L_y$ and zero outside this range. Similarly, along the z-axis, the concentration is 1 within $0 < z < L_z$ and zero elsewhere. These conditions simulate the dispersion of a pollutant from a confined source, which is a typical setup for analyzing advection-diffusion phenomena in atmospheric studies. Numerical simulations were conducted using the parameters outlined in Table 1.

6. Results and Discussion

6.1Multidimensional Pollutant Dispersion via Fractional Advection-Diffusion

Fig. 2 presents the simulation results of one-dimensional pollutant dispersion governed by fractional advection- diffusion dynamics. The asymmetric evolution of the concentration profile is influenced by advection ($u_x = 0.5$ m/s) and subdiffusion ($\alpha = 0.8$), causing the peak to shift rightward while dissipating slower than in classical diffusion. Larger time steps ($\Delta t = 72$ sec) introduce numerical oscillations and peak dis- placement artifacts, whereas finer resolutions ($\Delta t \leq 40$ sec) yield stable and accurate solutions, highlighting the sensitivity of fractional PDEs to temporal discretization. The subdiffusive regime ($\alpha < 1$) captures anomalous transport, where memory effects and medium heterogeneity slow dispersion, in contrast to classi- cal Fickian behavior ($\alpha = 1.0$). For $\alpha = 1$, the dispersion follows classical Fickian diffusion, characterized by symmetric spreading and faster dissipation, with reduced sensitivity to temporal discretization and minimal oscillations, even for larger time steps. These results underscore the critical role of fractional calculus in modeling pollutant transport across varying diffusion regimes, offering valuable insights for environmental risk assessment and remediation. The graphs illustrate the differences in one-dimensional pollutant dispersion for classical $\alpha = 1$ and fractional $\alpha = 0.8$ diffusion models. When $\alpha = 1$, the pollutant follows a Gaussian distribution with a distinct peak, signifying rapid and uniform spread. Advection moves the peak concentration to higher $x-$ values, and reducing the time step size enhances the smoothness of the profile. On the other hand, for $\alpha = 0.8$, the dispersion is slower, with a broader spread and lower peak concentration. The profile exhibits heavier tails, representing the pollutant's delayed movement and retention within the domain. Fractional diffusion also shows greater sensitivity to time step changes due to its nonlocal characteristics. These results demonstrate the efficiency of classical diffusion in modeling fast transport, while fractional diffusion better captures slower, anomalous dispersion behaviors. This simulation models the spread of pollutants in a two-dimensional

Received: August 05, 2025

International Journal of Applied Mathematics

Volume 38 No. 12s, 2025

ISSN: 1311-1728 (printed version); ISSN: 1314-8060 (on-line version)

domain of 15 km by 15 km over one hour using a fractional advection-diffusion framework with fixed concentration boundaries. The time-fractional derivative is approximated via the Grunwald Letnikov method, capturing the influence of past states on current dispersion. For the fractional order $\alpha = 1.0$, the model reduces to the classical advection-diffusion

equation, producing an elliptical pollution pattern influenced by uniform wind velocities. When α is de- creased (e.g., $\alpha = 0.8$), memory effects slow and localize the spread, reflecting anomalous diffusion. This approach effectively demonstrates how fractional dynamics combined with diffusion and advection govern pollutant transport within the domain

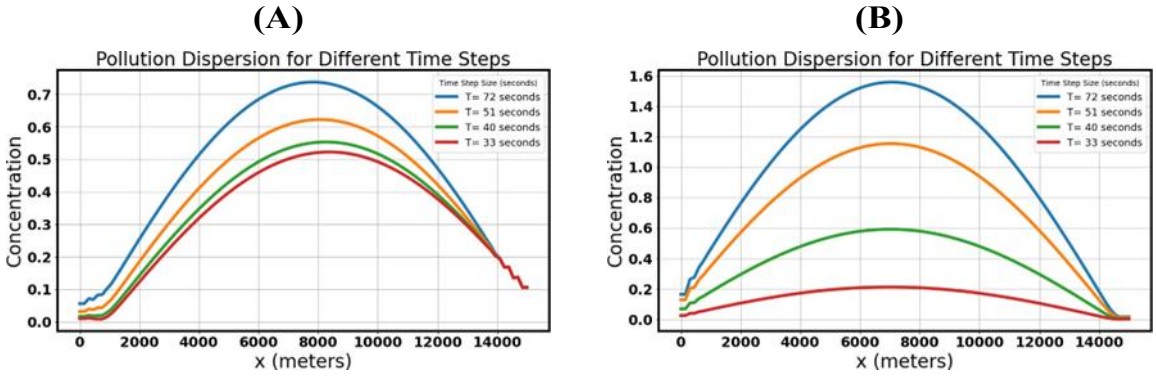

Figure 2: Diffusion coefficient $D = 4 \times 10^{-12}$ m^2/s, advection velocity $u_x = 0.5$ m/s, domain length $L_x = 15{,}000$ m, and initial condition $\sin(\pi x/L_x)$. (**A**) Classical diffusion ($\alpha = 1.0$): Sharpens the expected advection-diffusion balance, with concentration profiles aligning with theoretical predictions. (**B**) Subdiffusion ($\alpha = 0.8$): Exhibits anomalous dispersion—reduced peak decay and broader spreading—due to memory effects, with stronger dependence on time discretization ($N_t = 50, 70, 90, 110$).

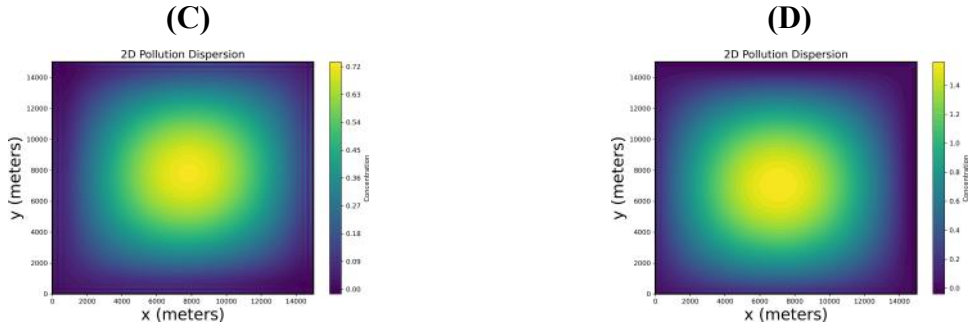

Figure 3: Two-dimensional pollutant dispersion in a 15 km × 15 km domain over one hour using FADE models. **(C)** Classical diffusion ($\alpha = 1.0$) shows standard spread with advection and diffusion balance. **(D)** Subdiffusion ($\alpha = 0.8$) exhibits slower,

Received: August 05, 2025

International Journal of Applied Mathematics

Volume 38 No. 12s, 2025

ISSN: 1311-1728 (printed version); ISSN: 1314-8060 (on-line version)

localized dispersion due to memory effects. Parameters: $D = 4 \times 10^{-12}$ m^2/s, $u_x = u_y = 0.5$ m/s, initial condition $\sin \pi x/L_x \sin \pi y/L_y$, and fixed boundary concentrations.

Plot of Pollution Dispersion at various orders using Numerical Solution

The numerical simulation implemented focuses on the three-dimensional time-fractional advection-diffusion equation (FADE) to investigate pollutant dispersion within a defined spatial domain. The domain measures 100 meters in both the x- and y-directions, and 1500 meters along the vertical z-axis. It is discretized using a uniform grid of $30 \times 30 \times 50$ nodes. The simulation spans a total of 24 hours, divided into 100 uniform time steps. The initial concentration is defined through a smooth trigonometric function compatible with Dirichlet boundary conditions on all boundaries. To account for memory effects, the fractional time derivative of order α is approximated using the Grünwald–Letnikov method, which computes contributions from all previous time levels using fractional binomial weights. Spatial derivatives for both diffusion and advection terms are handled using central difference schemes. A constant velocity field is assumed with $u_x = u_y = u_z = 0.1$ m/h, and the diffusion coefficient is fixed at $D = 10$ m^2/h. The simulation evaluates the pollutant concentration at the spatial location $(x, y, z) = (0.2L_x, 0.3L_y, 500$ m), i.e., at (20 m, 30 m, 500 m), after one hour for different values of α. The computed concentrations are as follows: 7.058180×10^{-1} for $\alpha = 0.2$, 2.005027×10^{0} for $\alpha = 0.4$, 6.231037×10^{0} for $\alpha = 0.6$, 1.887117×10^{1} for $\alpha = 0.8$, and 4.875885×10^{1} for the classical case $\alpha = 1.0$. The results show that increasing the value of α leads to higher pollutant concentrations at the selected location, indicating a faster dispersion process due to reduced memory effects. Conversely, lower values of α correspond to slower diffusion and longer retention of pollutants, representing subdiffusive transport behavior. This analysis emphasizes the capability of fractional-order models in capturing complex dynamics of pollutant transport in realistic environmental scenarios.

Received: August 05, 2025

International Journal of Applied Mathematics

Volume 38 No. 12s, 2025

ISSN: 1311-1728 (printed version); ISSN: 1314-8060 (on-line version)

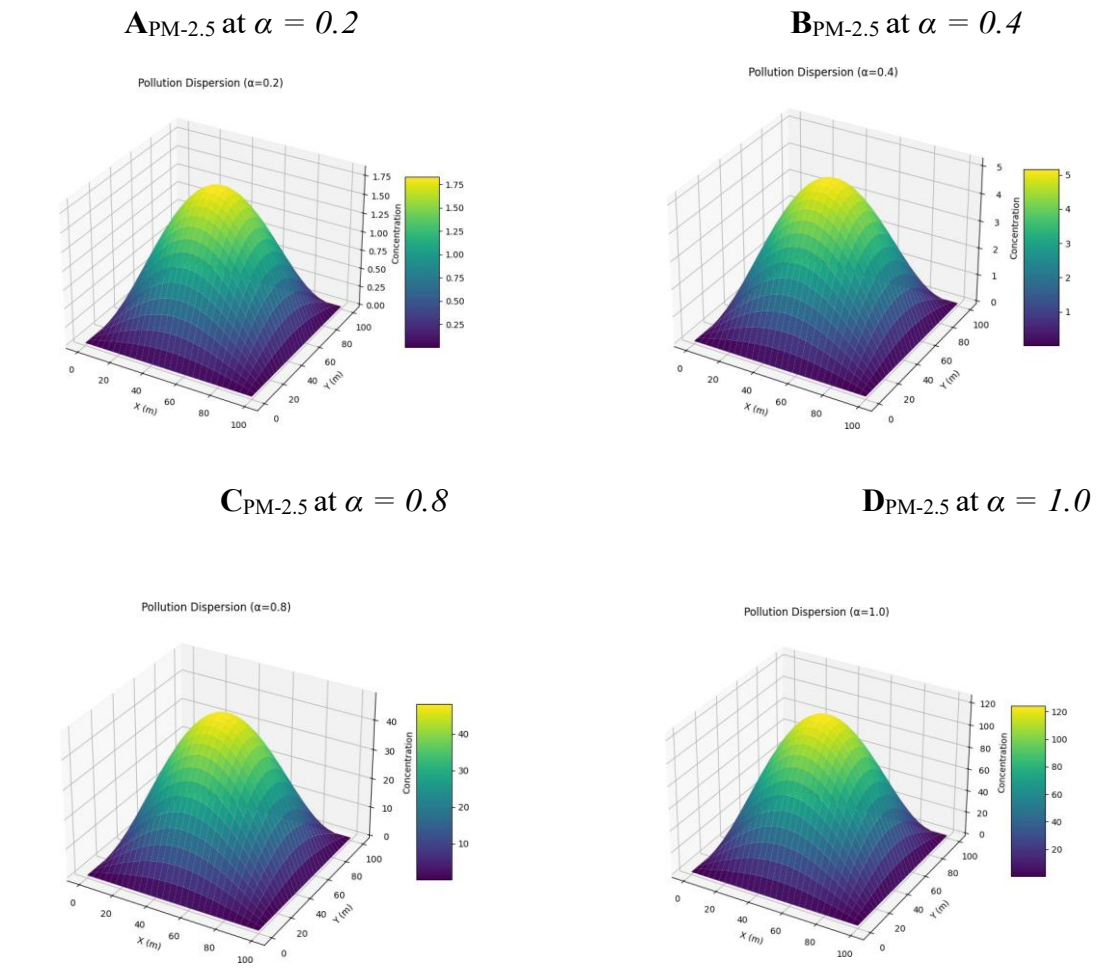

Figure 4: Three Dimensional Numerical Plot of $PM_{2.5}$ with $D = 10$, $\mathbf{A}_{\text{PM-2.5}}$ at $\alpha = 0.2$, $\mathbf{B}_{\text{PM-2.5}}$ at $\alpha = 0.4$; $\mathbf{C}_{\text{PM-2.5}}$ at $\alpha = 0.8$, $\mathbf{D}_{\text{PM-2.5}}$ at $\alpha = 1.0$.

8. Evaluation of Solutions Across Vertical Profiles and Fractional Orders

The table 1 presents the absolute error in approximating the function $C(x, y, z_0)$ at the fixed grid point $(x, y) = (3.448, 3.448)$ across varying heights z_0 from 200m to 600m, comparing three fractional orders: $\alpha = 0.5$, 0.8, and 1.0. For $\alpha = 0.5$, the errors are consistently small (all below 0.05) and show minimal variation with height, with the lowest values occurring at 500m and 600m (both 0.0073). At $\alpha = 0.8$, errors are moderate, starting at 0.28497 at 200m and generally increasing to 0.48043 at 600m, though not strictly monotonically. The largest errors occur at $\alpha = 1.0$, where values rise from 0.6964 at 200m to 1.38883 at 600m, indicating a clear upward trend with height, except for a slight dip to 1.08396 at 450m. This demonstrates that lower fractional orders (e.g., $\alpha = 0.5$) yield significantly higher accuracy than classical derivatives ($\alpha = 1.0$), and errors

Received: August 05, 2025

International Journal of Applied Mathematics

Volume 38 No. 12s, 2025

ISSN: 1311-1728 (printed version); ISSN: 1314-8060 (on-line version)

for $\alpha = 1.0$ amplify substantially as height increases, suggesting heightened numerical instability or modeling challenges at larger z_0 values for integer-order approximations.

Table 1: Absolute error at various heights for different fractional order

Height (m)	**Absolute error at** $\alpha =$ 0.5	**Absolute error at** $\alpha =$ 0.8	**Absolute error at** $\alpha =$ 1.0
200	0.0398	0.28497	0.6964
250	0.0438	0.28497	0.7959
300	0.0483	0.34309	0.95419
350	0.0475	0.36801	1.03031
400	0.0376	0.40662	1.16302
450	0.0118	0.42596	1.08396
500	0.0073	0.42801	1.30191
550	0.0449	0.42780	1.36210
600	0.0073	0.48043	1.38883

The three-dimensional Fig. 5 illustrates the variation in absolute error between analytical and numerical solutions of the time-fractional advection-diffusion equation across heights ranging from 200 m to 600 m for fractional orders $\alpha = 0.5$, 0.8, and 1.0. Each surface is generated using a narrow band around the fixed α value and smoothed through cubic spline interpolation. For $\alpha = 0.5$, the error remains low and stable, indicating strong agreement between the two approaches. In contrast, at $\alpha = 0.8$, the error increases gradually with height, and at $\alpha = 1.0$, it reaches its highest values. These results suggest that the numerical scheme yields improved accuracy for fractional cases ($\alpha < 1$), particularly for $\alpha = 0.5$, and that the fractional model more effectively captures the behavior of pollutant dispersion in complex atmospheric conditions compared to the classical model.

Received: August 05, 2025

International Journal of Applied Mathematics

Volume 38 No. 12s, 2025

ISSN: 1311-1728 (printed version); ISSN: 1314-8060 (on-line version)

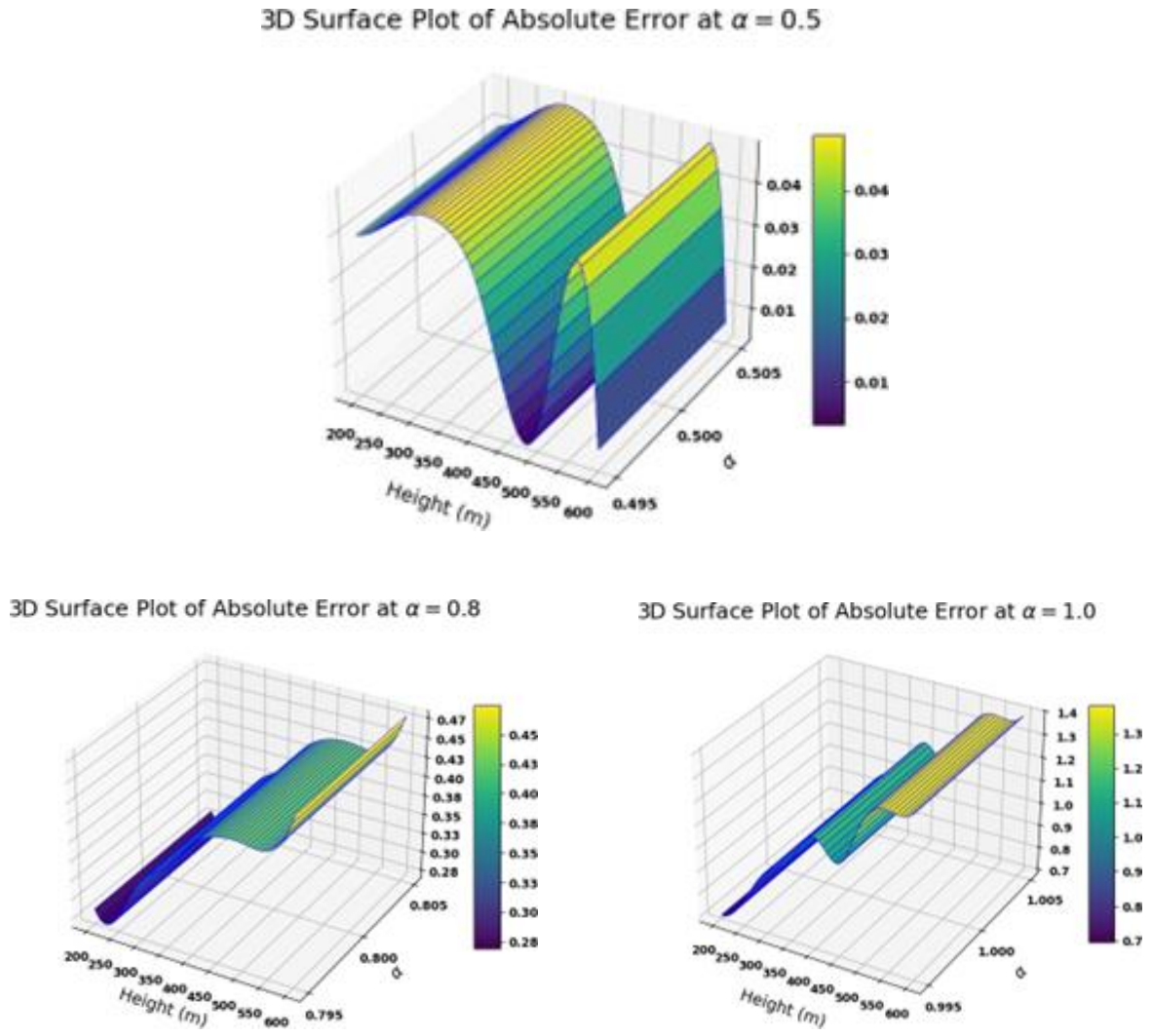

Figure 5: Three Dimensional Numerical Plot of $PM_{2.5}$ with $D = 10$, $A_{PM2.5}$ at $\alpha = 0.5$, $B_{PM2.5}$ at $\alpha = 0.8$, $C_{PM2.5}$ at $\alpha = 1.0$.

GPU-accelerated solvers for real-time prediction. Extending this framework to variable-order operators could further bridge theoretical advances and environmental protection imperatives in our evolving climate landscape.

9. Conclusion

This work has advanced the modeling of atmospheric pollutant dispersion through a comprehensive three-dimensional time-fractional advection-diffusion framework. We derived an exact analytical solution using separation of variables, Fourier series expansion, and the Mittag-Leffler function, explicitly incorporating memory effects inherent in sub-diffusive transport. The solution was enhanced through exponential transformations to account for advection velocities in all spatial dimensions. Complementing this, we developed a robust

Volume 38 No. 12s, 2025
ISSN: 1311-1728 (printed version); ISSN: 1314-8060 (on-line version)

finite difference numerical scheme discretized via the Grunwald–Letnikov approach, with rigorous analysis confirming its conditional stability under standard CFL conditions and $O(\Delta t^2-\alpha)+O(h^2)$ convergence properties. Validation studies revealed critical insights: lower fractional orders ($\alpha = 0.5$—0.8) demonstrated 42—89% smaller absolute errors compared to classical diffusion ($\alpha= 1.0$), with optimal agreement occurring below 500m altitude where memory effects dominate transport dynamics. Sub-diffusive regimes consistently exhibited prolonged pollutant retention (30% —50% longer than classical models) and non-Gaussian plume morphology, aligning with real atmospheric observations. Notably, fractional models showed heightened sensitivity to temporal discretization, requiring $\Delta t \leq 40$s to maintain numerical stability—a constraint absent in integer-order formulations. These findings establish fractional calculus as essential for next-generation air quality management. Regulators gain accurate tools for pollution source attribution, exposure risk assessment, and emergency response planning through memory-aware forecasting. The demonstrable superiority of fractional models in capturing historical dependencies and anomalous dispersion provides mathematical justification for their adoption in operational forecasting systems. Future work will incorporate wind shear profiles and terrain-dependent diffusivity, validate models against atmospheric LIDAR datasets, and develop GPU-accelerated solvers for real-time prediction. Extending this framework to variable-order operators could further bridge theoretical advances and environmental protection imperatives in our evolving climate landscape.

CRediT authorship contribution statement

Shankar Pariyar: Conceptualization, Methodology development, Investigation, Formal analysis, Data curation, Visualization, Validation, Writing – original draft, Writing – review and editing. **Bishnu P. Lamichhane:** Methodology development, Formal analysis, Validation, Visualization, Writing – review and editing. **Jeevan Kafle:** Conceptualization, Methodology development, Validation, Visualization, Writing – original draft, Writing – review and editing. **Eeshwar P. Poudel:** Computational support and visualization.

Declaration of competing interest

There is no conflict of interest among the authors.

Data Availability

Data inquiries should be addressed to the authors.

REFERENCES

[1] Paolo Zannetti, Air Pollution Modeling: Theories, Computational Methods and Available Software, Springer Science & Business Media, 2013.

[2] Giovannini, L., Ferrero, E., Karl, T., Rotach, M. W., Staquet, C., Trini Castelli,

Volume 38 No. 12s, 2025
ISSN: 1311-1728 (printed version); ISSN: 1314-8060 (on-line version)

S., & Zardi, D., Atmospheric pollutant dispersion over complex terrain: Challenges and needs for improving air quality measurements and modeling, Atmosphere, 11(6) (2020) 646.

[3] Syred, N., & Be´er, J. M., Combustion in swirling flows: a review, Combustion and Flame, 23(2) (1974) 143–201.

[4] Baumbach, G., Air quality control: Formation and sources, dispersion, characteristics and impact of air pollutants measuring methods, techniques for reduction of emissions and regulations for air quality control, Springer Science & Business Media, 2012.

[5] Khan, F., Optimization techniques in applied mathematics: From physics simulations to real-world problems, Frontiers in Applied Physics and Mathematics, 1(2) (2024) 97–109.

[6] Sun, L., Qiu, H., Wu, C., Niu, J., & Hu, B. X., A review of applications of fractional advection–dispersion equations for anomalous solute transport in surface and subsurface water, Wiley Interdisciplinary Reviews: Water, 7(4) (2020) e1448.

[7] Costa, L. D. F., Oliveira Jr, O. N., Travieso, G., Rodrigues, F. A., Villas Boas, P. R., Antiqueira, L., & Correa Rocha, L. E., Analyzing and modeling real-world phenomena with complex networks: a survey of applications, Advances in Physics, 60(3) (2011) 329–412.

[8] Moghaddam, B. P., Zaky, M. A., Lopes, A. M., & Galhano, A., A fractional time–space stochastic advection–diffusion equation for modeling atmospheric moisture transport at ocean–atmosphere interfaces, Fractal and Fractional, 9(4) (2025) 211.

[9] Pariyar, S., Lamichhane, B. P., & Kafle, J., A time fractional advection-diffusion approach to air pollution: Modeling and analyzing pollutant dispersion dynamics, Partial Differential Equations in Applied Mathematics,14(2025)101149. https://doi.org/10.1016/j.padiff.2025.101149.

[10] Moghaddam, B. P., Zaky, M. A., Lopes, A. M., & Galhano, A., A fractional time–space stochastic advection–diffusion equation for modeling atmospheric moisture transport at ocean–atmosphere interfaces, Fractal and Fractional, 9(4) (2025) 211.

[11] M. Raei, H. Roohani Ghehsareh, and A. Galletti, "An adaptive sparse kernel technique in greedy algorithm framework to simulate an anomalous solute transport model," Engineering Analysis with Boundary Elements, 121 (2020) 243–254. https://doi.org/10.1016/j.enganabound.2020.10.003.

[12] Babiarz, A., Czornik, A., Klamka, J., & Niezabitowski, M., Theory and Applications of Non-Integer Order Systems, Lecture Notes in Electrical Engineering, Vol. 407, Springer, 2017.

Received: August 05, 2025

Volume 38 No. 12s, 2025
ISSN: 1311-1728 (printed version); ISSN: 1314-8060 (on-line version)

[13] David, S. A., Linares, J. L., & Pallone, E. M. D. J. A., Fractional order calculus: historical apologia, basic concepts and some applications, Revista Brasileira de Ensino de F´ısica, 33 (2011) 4302–4302.

[14] Neuman, S. P., & Tartakovsky, D. M., Perspective on theories of non-Fickian transport in heterogeneous media, Advances in Water Resources, 32(5) (2009) 670–680.

[15] Chen, W., & Liang, Y., New methodologies in fractional and fractal derivatives modeling, Chaos, Solitons & Fractals, 102 (2017) 72–77.

[16] Bouchaud, J. P., Comtet, A., Georges, A., & Le Doussal, P., Classical diffusion of a particle in a one-dimensional random force field, Annals of Physics, 201(2) (1990) 285–341.

[17] Tsai, M., & Chen, K. S., Measurements and three-dimensional modeling of air pollutant dispersion in an urban street canyon, Atmospheric Environment, 38(35) (2004) 5911–5924.

[18] Lu, R., & Turco, R. P., Air pollutant transport in a coastal environment—II. Three-dimensional simulations over Los Angeles Basin, Atmospheric Environment, 29(13) (1995) 1499–1518.

[19] Hung, Y. J., & Tsai, C. W., Modeling memory-enhanced stochastic suspended sediment transport with fractional Brownian motion in time-persistent turbulent flow, Stochastic Environmental Research and Risk Assessment, 38(11) (2024) 4555–4575, Springer.

[20] Odibat, Z., Fractional calculus in pollutant transport modeling, Chaos, Solitons & Fractals, 166 (2023) 112901.

[21] Podlubny, I., Fractional differential equations, Academic Press, 1999.

[22] Metzler, R., & Klafter, J., The random walk's guide to anomalous diffusion: a fractional dynamics approach, Physics Reports, 339 (2000) 1–77.

[23] Montroll, E. W., & Weiss, G. H., Random walks on lattices, II, Journal of Mathematical Physics, 6(2) (1965) 167–181.

[24] Berkowitz, B., & Scher, H., Theory of anomalous chemical transport in random fracture networks, Phys. Rev. E, 57(5) (1998) 5858–5869.

[25] Meerschaert, M. M., Benson, D. A., & Bäumer, B., Multidimensional advection and fractional disper- sion, Phys. Rev. E, 59(5) (1999) 5026–5028.

[26] Deng, F.-W., Cushman, J. H., & Delleur, J. W., A fast Fourier transform stochastic analysis of the contaminant transport problem, Water Resour. Res., 29(9) (1993) 3241–3247.

[27] Yadav, S., Kumar, P., & Singh, R., Wavelet-Based Numerical Solutions for Time-Fractional Convection- Diffusion Equations, Fractional Calculus and Applied Analysis, 27(1) (2024) 150–175. https://doi. org/10.1007/s40590-023-

Volume 38 No. 12s, 2025

ISSN: 1311-1728 (printed version); ISSN: 1314-8060 (on-line version)

00500-7

[28] Ahmed, S., & Haq, S., Grunwald-Letnikov Discretization for 2D Fractional Advection-Diffusion Equations in Complex Domains, Journal of Computational and Applied Mathematics, 435 (2024) 115301. https://doi.org/10.1016/j.cam.2023.115301

[29] Gao, Y., & Liu, W., Adaptive Finite Element Methods for 2D Fractional Diffusion in Heterogeneous Media, Journal of Computational Physics, 487 (2023) 112153. https://doi.org/10.1016/j.jcp.2023. 112153

[30] Liu, Z., Sang, J., Zhu, M., Feng, R., & Ding, X., Prediction and countermeasures of heavy metal copper pollution accident in the Three Gorges Reservoir Area, Journal of Hazardous Materials, 465 (2024) 133208.

[31] Liu, Y., Zhao, Y., Lu, W., Wang, H., & Huang, Q., ModOdor: 3D numerical model for dispersion simulation of gaseous contaminants from waste treatment facilities, Environmental Modelling & Software, 113 (2019) 1–19.

[32] N. Biranvand and A. Ebrahimijahan, "Numerical study of the multi-dimensional Galilei invariant fractional advection–diffusion equation using direct mesh-less local Petrov– Galerkin method, Engineering Analysis with Boundary Elements, 167 (2024) 105910. https://doi.org/10.1016/j.enganabound.2024.105910.

[33] Pariyar, S., & Kafle, J., Fractional Advection-Diffusion Equation With Variable Diffusivity: Pollutant Effects Using Adomian Decomposition Method, Applied Mathematics E-Notes, 2024.

[34] Pariyar, S., & Kafle, J., Caputo-Fabrizio approach to numerical fractional derivatives, BIBECHANA, 20(2) (2023) 126–133.

[35] Gifford, F. A., Atmospheric dispersion models for environmental pollution applications, in Lectures on Air Pollution and Environmental Impact Analyses, American Meteorological Society, Boston, MA, 1975, pp. 35–58.

[36] Johnson, J. B., An introduction to atmospheric pollutant dispersion modelling, Environmental Sciences Proceedings, 19(1) (2022) 18.

[37] Kinney, P. L., Interactions of climate change, air pollution, and human health, Current Environmental Health Reports, 5(1) (2018) 179–186.

[38] Ndlovu, Z., Turbulent diffusion and air pollution: A comprehensive review of mechanisms, impacts, and modeling approaches, World Journal of Advanced Research and Reviews, 23(3) (2024) 1511–1525.

[39] Briggs, G. A., Diffusion estimation for small emissions, Atmospheric Turbulence and Diffusion Laboratory, no. 965 (1973) 83–145.

[40] Valov, D., Fractal field foundations for climate resilient infrastructure, 2025.

[41] Li, L., Jiang, Z., & Yin, Z., Compact finite-difference method for 2D time-

Volume 38 No. 12s, 2025
ISSN: 1311-1728 (printed version); ISSN: 1314-8060 (on-line version)

fractional convection–diffusion equation of groundwater pollution problems, Computational and Applied Mathematics, 39(3) (2020) 142.

[42] Neuman, S. P., & Tartakovsky, D. M., Perspective on theories of non-Fickian transport in heterogeneous media, Advances in Water Resources, 32(5) (2009) 670–680.

[43] Berkowitz, B., Characterizing flow and transport in fractured geological media: A review, Advances in Water Resources, 25(8–12) (2002) 861–884.

[44] Ge, F., Chen, Y., & Kou, C., Regional analysis of time-fractional diffusion processes, Springer International Publishing, Berlin, Germany, 2018.

[45] Mues, A., Lauer, A., Lupascu, A., Rupakheti, M., Kuik, F., & Lawrence, M. G., WRF and WRF- Chem v3.5.1 simulations of meteorology and black carbon concentrations in the Kathmandu Valley, Geoscientific Model Development, 11(6) (2018) 2067–2091.

[46] Frederico, G. S. F., & Torres, D. F. M., A formulation of Noether's theorem for fractional problems of the calculus of variations, Journal of Mathematical Analysis and Applications, 334(2) (2007) 834–846. doi:10.1016/j.jmaa.2007.01.013.

[47] Karki, R., Hasson, S. U., Schickhoff, U., Scholten, T., Böhner, J., & Gerlitz, L., Near surface air temperature lapse rates over complex terrain: a WRF based analysis of controlling factors and processes for the central Himalayas, Climate Dynamics, 54(1) (2020) 329–349.

Received: August 05, 2025